Volume 5
Number 11
November 2025
Pages 1175–1264

Environmental Science
Atmospheres

rsc.li/esatmospheres

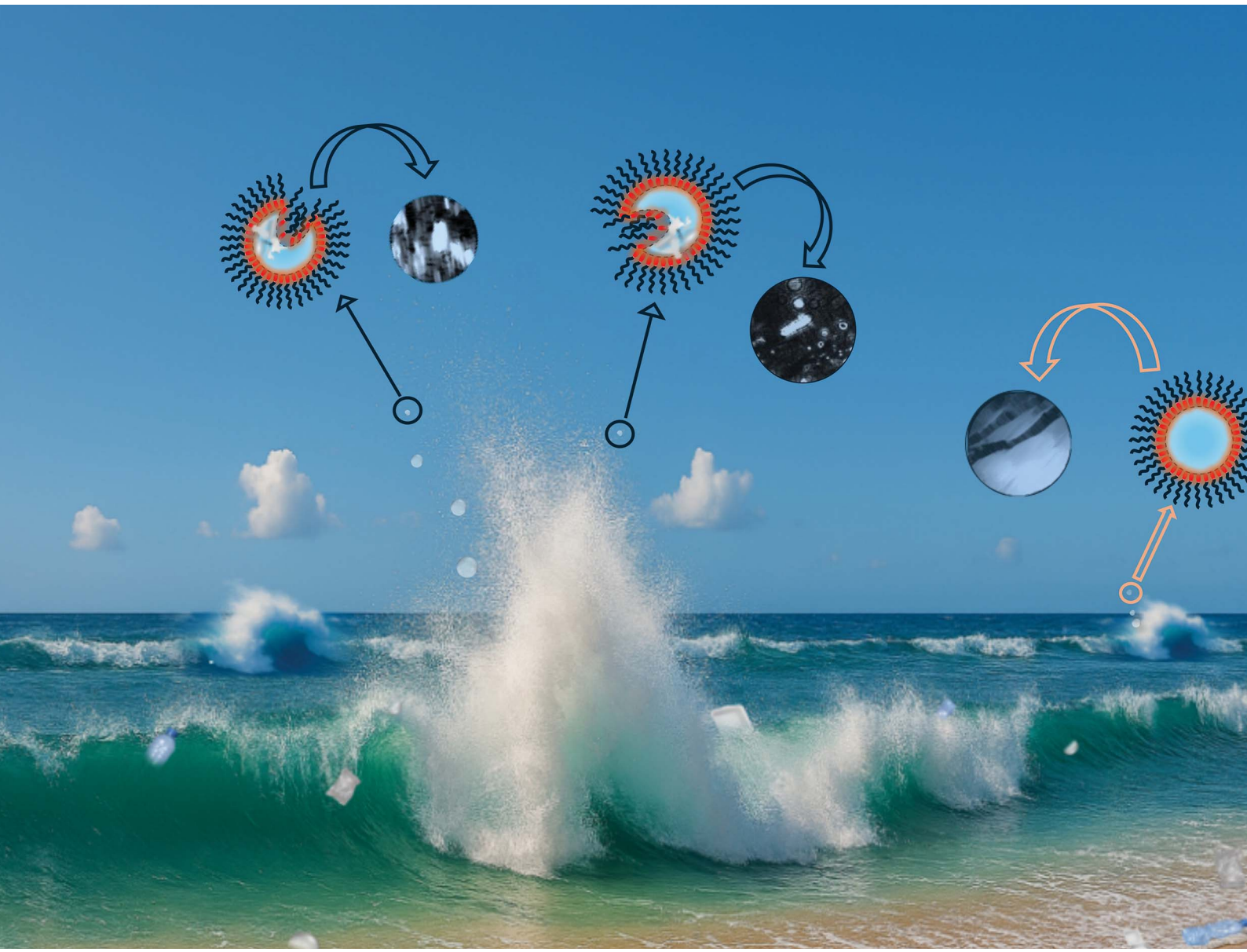

ISSN 2634-3606

ROYAL SOCIETY OF CHEMISTRY

PAPER
Heather C. Allen *et al.*
Nanoplastic–lipid interactions at marine relevant interfaces: implications for atmospheric chemistry

Environmental Science: Atmospheres

ROYAL SOCIETY OF CHEMISTRY

PAPER

View Article Online
View Journal | View Issue

Cite this: *Environ. Sci.: Atmos.*, 2025, **5**, 1180

Nanoplastic–lipid interactions at marine relevant interfaces: implications for atmospheric chemistry

Shamma Jabeen Proma,[a] Biswajit Biswas,[a] Shahin Ahmed Sujon,[b] Kyle J. Moor,[b] Janice Brahney[c] and Heather C. Allen *[a]

Nanoplastics—originating from the fragmentation of macro- and micro plastic debris or direct industrial sources—have recently been recognized as an emerging class of marine pollutants with persistent oceanic presence. These tiny colloidal particles can potentially accumulate near the ocean surface owing to their buoyant and hydrophobic nature, positioning themselves within the sea surface microlayer (SSML), a biologically active interfacial zone enriched in lipids, proteins, and polysaccharides that shapes the chemical composition of sea spray aerosols (SSAs) generated during wave breaking events. In this study, we investigated the interfacial interactions between aged (mimicking solar UV wavelengths) polystyrene nanoplastics and a marine-representative lipid, palmitic acid (a dominant fatty acid in the ocean SSML and a known SSA constituent), using a combination of surface pressure-area isotherms, Brewster angle microscopy (BAM), and infrared reflection–absorption spectroscopy (IRRAS). The results demonstrate that nanoplastics dispersed in a seawater-proxy subphase solution significantly disrupts the structural integrity and morphology of palmitic acid films by altering intermolecular cohesion. Additionally, spectroscopic evidence suggests that these disruptions are predominantly mediated by cation–driven interactions at the carboxylate headgroup region, while the lipid hydrophobic core conserves its packing orientation. Such findings indicate that nanoplastics incorporated into SSAs can modify the surface organic film morphology during their atmospheric flight time, potentially altering aerosol mechanical stability, hygroscopicity, and cloud condensation nuclei (CCN) activity—processes that ultimately influence aerosol–cloud interactions and climate-relevant mechanisms.

Received 27th June 2025
Accepted 5th September 2025

DOI: 10.1039/d5ea00075k

rsc.li/esatmospheres

Environmental significance

This research highlights the potential of nanoplastics in modifying the chemical properties of marine–relevant interfaces that are critical in mediating ocean–atmosphere interactions. As plastic debris continues to fragment and accumulate in marine environments, nanoplastics are increasingly likely to interact with the diverse organic materials within the sea surface microlayer (SSML), disrupt natural air–sea exchange processes, and affect pollutant transport. Given that SSML serves as a primary source for sea spray aerosol (SSA) production, such interactions could influence the aerosol morphology, chemical composition, and cloud-nucleating potential, carrying broader consequences for atmospheric chemistry, cloud formation, and Earth's radiative balance. The experimental findings underscore the importance of considering nanoplastics as active agents in ocean–atmosphere coupling and their potential role in climate-relevant processes.

1 Introduction

Since the onset of large-scale production of synthetic plastics back in the 1950s, the plastic manufacturing industry has experienced rapid worldwide growth. Global plastic production exceeded 413 million metric tons in 2023, and a significant portion enters the oceans annually through riverine discharge, direct dumping, and atmospheric deposition.[1] Over time, physical, chemical, and biological weathering processes degrade larger plastic debris into microplastics (1 μm to 5 mm) and eventually nanoplastics (<1 μm), forming a continuum of particulate pollution that infiltrates every marine compartment, from surface waters to deep-sea sediments.[1,2] In addition to originating from the breakdown of larger debris, micro- and nanoplastics are also intentionally manufactured for use in personal care products, medical applications, printing ink and electronics.[1,2] These engineered particles can enter marine environments *via* municipal wastewater systems, where their diminutive size allows them to evade standard filtration and detection techniques.[3]

A 2015 study based on field sampling and global models estimates that the surface oceans may host up to 51 trillion

[a]*Department of Chemistry & Biochemistry, The Ohio State University, USA. E-mail: allen@chemistry.ohio-state.edu*

[b]*Utah Water Research Laboratory, Department of Civil and Environmental Engineering, Utah State University, USA*

[c]*Department of Watershed Sciences, Utah State University, USA*

microplastic particles, with 200 mm being the upper size limit of the fragments.[4,5] Quantitatively, micro- and nanoplastic deposition into the marine environment has been calculated to be approximately 25 million metric tons or mega tons, Mt, per year, based on parameters such as measured atmospheric deposition rates in remote areas and the global ocean surface area.[1] A significant fraction of this input likely falls within the nano- and submicron size range, although direct measurements remain limited due to technical challenges.[6,7]

While early studies primarily focused on microplastic pollution, there is now growing evidence that nanoplastics constitute a substantial yet largely invisible component of the marine plastic burden. These nanosized plastic debris are extremely difficult to quantify, owing to analytical limitations, their tendency to aggregate, sedimentation processes and the difficulty in distinguishing synthetic nanomaterials from natural colloidal particles. Nevertheless, both modeling and field-based research now confirm the widespread presence of nanoplastics across diverse aquatic environments. For instance, nanoplastic concentrations as high as $\sim$0.6 mg L^{-1} have been reported in remote Swedish freshwater systems, highlighting their global ubiquity even in regions far from direct pollution sources.[8] The findings are consistent with other recent studies that have detected various nanoplastic morphologies—including nanofibers, flakes, and spheres—composed of common polymers such as polystyrene, polyethylene terephthalate, and nylon along marine coastlines in China, South Korea, the United States, and the Gulf of Mexico.[6]

Among the various oceanic compartments, the sea surface microlayer (SSML), a thin, gelatinous interface spanning the top $\sim$1–1000 μm of the ocean, is emerging as a critical accumulation zone for nanoplastics.[2] Enriched in organic compounds such as lipids, proteins, polysaccharides, and exopolymeric substances, the SSML acts as the ocean's biological and chemical "skin", playing a vital role in regulating gas exchange, pollutant dynamics, and aerosol production.[9] Recent studies report that micro- and nanoplastics are consistently enriched in the SSML relative to the underlying bulk waters, sometimes by a factor of three.[10] The presence of nanoplastics in this layer could disrupt its natural physicochemical properties, thereby altering air–sea interactions. Importantly, preferential accumulation of these plastics at the air–sea boundary also raises critical concerns about subsequent transfer into the atmosphere.

The transfer of nanoplastics from ocean to atmosphere through aerosolization is an emerging frontier in marine plastic research with evidence showing that sea spray aerosols (SSAs) formed by wave breaking and bubble bursting can entrain nanoplastics from the surface ocean and inject them into the atmosphere.[2,11] At the global scale, estimates for such ocean-to-air plastic fluxes vary widely, with emission ranges for microplastics spanning 0.02 to 7.4 Mt $year^{-1}$, and a central estimate of $\sim$0.1 Mt $year^{-1}$ derived from mechanistic models.[12] Although nanoplastic emissions are presumed to be smaller and more uncertain, their hydrophobicity and buoyancy can potentially enable complex and variable behavior at the ocean surface. Harb *et al.* in their 2023 study systematically parameterized the aerosolization process, showing that smaller particles (<10 μm) are more efficiently aerosolized and polystyrene nanoplastics of size $\sim$500 nm in particular were aerosolized with an enrichment factor up to 19-fold compared to the underlying bulk seawater.[11]

The sea spray aerosols represent one of the largest natural aerosol sources globally and play a dual role in climate: directly by scattering and absorbing solar radiation, and indirectly by acting as cloud condensation nuclei (CCN) and ice-nucleating particles (IN).[13,14] The atmospheric impact of SSA relies strongly on surface composition and phase state, properties that are dependent on the SSML from which they originate.[15–18] For example, SSAs generated during seasonal phytoplankton bloom contain higher organic enrichment within the aerosol droplets such that the competition for space at the SSA surface is high due to the surface activity of such marine-derived organic compounds.[13] These marine organics are known to form a film at the surface of SSA with a saline aqueous core much like the formation of a reverse micelle.[13] The small size, hydrophobicity, and tendency of nanoplastics to accumulate at or near the water interfaces position them with the ability to disrupt the morphology of the natural surfactant film at the SSA surface during their atmospheric flight time. Such perturbation could alter mechanical stability and film packing at the SSA surface, which would essentially affect its gas and water uptake, light scattering, and the ability to serve as cloud condensation nuclei.[19] This possibility is especially concerning given the vital role marine aerosols play in regulating Earth's radiation balance and cloud dynamics.[19]

Despite the potential for nanoplastics to accumulate in the SSML and alter the SSA composition and structure, their behavior in the air–aqueous interface remains poorly characterized. In particular, the fundamental interactions between nanoplastics and surface-active marine organic molecules, that are highly relevant to aerosol chemistry, are not well understood.[13,20] Understanding how nanoplastics influence their organization, chemistry, and dynamics is essential to predicting the broader environmental consequences of plastic pollution. Among these surface-active compounds in SSML, long-chain saturated fatty acids, particularly palmitic acid, are among the most abundant.[21] Palmitic acid (PA), produced by phototrophic algae, marine zooplankton, bacteria, and degradation of organic matter, contributes significantly to the organic content of marine surface microlayers.

PA monolayers are known for forming highly ordered two-dimensional films that undergo phase transitions under compression to different surface densities; these resulting phases are also sensitive to changes in temperature, pH, ionic strength, and cation type.[13] Because of its ubiquity in the ocean environment and well-characterized interfacial behavior, palmitic acid serves as an excellent model for studying the lipid–nanoplastic interactions at marine aerosol interfaces and the SSA film behavior during their atmospheric flight time can be represented by 2D Langmuir compression isotherms.[22] The SSA droplets undergo continuous evaporation in the atmosphere, which reduces the aqueous core volume and forces the surface-active film to occupy a progressively smaller interfacial area. This process is directly analogous to monolayer compression in

a Langmuir trough—the droplet surface shrinks, but the same number of surfactant molecules remain at the interface, increasing surface pressure.[13] In this study, we employed a multidisciplinary approach, combining Brewster angle microscopy (BAM) and infrared reflection–absorption spectroscopy (IRRAS) with Langmuir surface pressure–area isotherms to explore how weathered polystyrene nanoplastics perturb PA film morphology and chemically interact with the marine lipid molecules under environmentally relevant conditions designed to simulate extreme nanoplastic pollution scenarios. By systematically unraveling the nanoscale interaction mechanisms, our findings aim to advance the field's understanding of how nanoplastics influence the properties of sea spray aerosols that can potentially impact climate-relevant processes.

2 Materials & methods

2.1 Materials

Commercial polystyrene nanospheres of 100 nm diameter were purchased from MilliPoreSigma (dispersed in deionized water with a 2 wt% solid concentration, CAS number 9003-53-6) and UV-aged. According to the supplier's technical specifications, the pristine nanospheres carry a negative surface charge owing to the presence of surface sulfate groups from the polymerization reaction initiator. To simulate solar weathering, the commercial nanoplastics were then subjected to laboratory aging under conditions that replicate 2 months of solar UV exposure and the full procedure with appropriate discussion can be found in previous publications.[23,24] Palmitic acid ($C_{16}H_{32}O_2$, PA, ≥99%, Sigma-Aldrich) was used as received without further purification and dissolved in chloroform (HPLC Grade, Fisher Scientific) at a concentration of ~1 mM. For preparing a ocean water mimic to model marine interfaces, calcium chloride dihydrate (Certified ACS, Fisher Chemical) was used as received and sodium chloride (Certified ACS, Fisher Chemical) was used after baking for approximately 10 hours in a furnace at 650 °C to remove residual impurities.

2.2 Chemical and morphological features of the UV-aged nanoplastics

The UV-aged PS nanoplastics exhibited substantial changes in both their physical and chemical properties compared to the pristine or commercial version; a detailed discussion can be found in our previous research.[23] Briefly, the UV-simulated solar weathering caused the PS nanoplastics to degrade from their original uniform, spherical shape into fibrous or flaky fragments. This deformation also made the aged PS nanoplastics more prone to agglomeration, as evidenced by their clustered appearance in atomic force microscopy (AFM) images and the reduced zeta potential of their aqueous suspensions compared to the pristine counterparts. A portion of the aged nanoplastics also showed spectral changes that are indicative of polymer degradation, potentially due to dissociation or chain scission. However, a large portion of the aged PS nanoplastics gave identical spectra to the pristine version.

2.3 Sample preparation

The aqueous solution mimicking seawater (ionic strength = 497 mM) was prepared with constant marine water concentrations of 467 mM NaCl and 10 mM $CaCl_2$, and the solution pH (~8.3) was adjusted by adding microliter aliquots of 0.345 M NaOH solution prepared by dissolving sodium hydroxide pellets (98% extra pure, ACROS Organics) in ultrapure water. Given that recent studies have detected nanoplastic concentrations of 0.6 mg L^{-1} in remote freshwater systems far from direct pollution sources, we have chosen about 8 times of that for the experimental concentration in our studies to mimic highly polluted regions such as enclosed or semi-enclosed marine coastal areas that are influenced by population centers, river discharge, and agricultural runoff.[8] Moreover, as polystyrene nanoplastics have been shown to be enriched in sea spray aerosols by up to 19-fold relative to the underlying bulk seawater, we consider our chosen concentration of ~5 mg L^{-1} to be both environmentally relevant and representative of conditions within aerosol droplets formed during wave-breaking events in polluted marine regions.[11] For our studies, the PS nanoplastics-aqueous solutions were freshly prepared by mixing appropriate amounts of PS nanoplastics-water dispersion stock with the water or salt solution before each experiment.

2.4 Dynamic light scattering & zeta potential

Dynamic light scattering (DLS) measures fluctuations in scattered light caused by the Brownian motion of nanoparticles in suspension, providing information on their size distribution. On the other hand, zeta potential quantifies the surface charge of nanoparticles by measuring the electrical potential at the interface between the solid surface and the surrounding liquid. The DLS and zeta potential measurements for the 5 mg L^{-1} PS nanoplastics in aqueous or salt solutions were performed in the Zetasizer Nano-ZS (Malvern) following standard procedures. The data presented is an average of multiple trials where each trial is an average of 3 measurements (20 runs per measurement).

2.5 Langmuir surface pressure–area isotherms

Surface pressure–area (π–A) isotherms represent the graphical relationship between the pressure exerted by a Langmuir monolayer/film adsorbed on a liquid surface and the area available to it. This technique measures the difference in surface tension of an aqueous solution in absence (γ_0) and presence (γ_f) of the Langmuir film covering the surface *i.e.*, $\pi = (\gamma_0) - (\gamma_f)$. The surface pressure changes as the area available per molecule in the film decreases under constant symmetric compression. The changing shape of the π–A curve gives information on surface organization and structural changes of the film on subphase solutions under different surface densities and reveal its packing structure, compressibility, and phase transition behaviors.[21,25] At large areas, where the molecular packing is low, the surface pressure is generally low. However, as the molecules are compressed and the available surface area decreases, the surface pressure increases. At a certain point,

a phase transition may occur, causing the film packing to shift from a gas-like state to a more solid-like state, leading to a sharp increase in surface pressure. The π–A isotherms were performed in a Teflon Langmuir trough fitted with movable Delrin barriers (KSV NIMA, Biolin Scientific) using a platinum Wilhelmy plate. Before each trial, the platinum plate, trough and barriers were thoroughly cleansed with reagent alcohol (Histological grade, Fisher Scientific) and nanopure water. To remove residual organics, the platinum plate was further flamed in a Bunsen burner until the plate glowed red hot. During experiments, before spreading the palmitic acid surfactant solution prepared in chloroform on the PS nanoplastics-salt solutions, the surface cleanliness was checked by sweeping the barriers at the maximum speed to ensure the surface pressure value remained $\leq$0.40 mN m^{-1}. This reveals that the bare PS nanoplastic-salt solutions do not contain any significant amount of impurity and the nanoplastics mostly solubilize in the solution instead of forming macro clusters at the air–aqueous interface that could change surface pressure significantly. A 100 μL Hamilton micro syringe was used to spread the surfactant solution dropwise onto the nanoplastics-salt solutions to form a thin film and the chloroform was allowed to evaporate for the next 10 min. The films were then symmetrically compressed at a constant speed of 2.5 mm min^{-1} per barrier, the lower mechanical compression rate enabling higher metastability to the isotherms under the non-equilibrium experimental condition.[26] The π–A isotherms were recorded at 20 $\pm$ 0.6 °C and a relative humidity of 31 $\pm$ 10%. The average of three isotherms were plotted using the Origin software (OriginPro 9) following average/merge multiple curves function technique. The standard deviation stayed within $\pm$1 Å^2 per molecule for the X axis/mean molecular area, and less than $\pm$0.5 mN m^{-1} in general and $\sim$ $\pm$3 mN m^{-1} in collapse phase for Y axis/surface pressure.

2.6 Brewster angle microscopy (BAM)

The Brewster angle microscope is a non-invasive imaging technique generally used to study thin films/partial films spread on aqueous solutions. This technique provides information on the structural and optical properties of the Langmuir films upon changes in surface density, subphase solution composition, temperature *etc.* The instrumentation is based on the light reflection properties of water surfaces, with the p-polarized light theoretically having null and in practice minimal reflectivity when incident on water surface at its Brewster angle.[27] Presence of amphiphilic compounds such as palmitic acid surfactants on water surface changes the interfacial composition and optical properties, with the reflected light providing information on molecular arrangements, surface irregularities due to adsorption with a clear contrast for imaging. Briefly, the home-built BAM in the Allen lab includes a $\sim$1 mW HeNe laser that emits a plane-polarized light at 543 nm wavelength (Research Electro-Optics) and a Glan-laser calcite polarizer further purifies the incident light to vertically linearly or p-polarized light (GL-10A, Thorlabs). The reflected light from the sample surface is captured and magnified by a 10$\times$ infinity-corrected objective lens with 17.5 mm working distance (CF160 Tu Plan EPI, Nikon Instruments). A 200 mm focal length tube lens (MXA22018, Nikon Instruments) is then used to focus the collimated beam onto a back-illuminated EMCCD camera (ProEM-HS: 512BX3, Teledyne Princeton Instruments). The optical assembly and camera are mounted on a custom-made goniometer that fixes the incidence angle to $\sim$53.1° *i.e.*, the Brewster angle of water. The instrument is capable of differentiating between surfactant aggregates of sizes around $\sim$10 μm and has a spatial resolution of less than 2 μm. The fixed camera position and constant working distance of the objective lens also helps in visualizing the temporal mobility of surfactant aggregates or monolayers within a defined region at the focal plane. For the experiments, a drop-casting method following previous research was used for spreading the lipid films on the bare saline and PS nanoplastics-salt solutions in acid-cleaned Petri dishes.[23,28] The average area occupied by a single molecule of PA *i.e.*, the mean molecular area (MMA), and the corresponding volume of the 1 mM solution required to spread dropwise were calculated based on the area of the Petri dishes. This calculation was done to replicate the distinct phases of the isotherms, which exhibit different packing structures due to the varying number density of the available PA molecules on the surface. Notably, in this drop-casting method, the interface reaches a non-equilibrium stability, and the information provided in terms of fundamental interactions or adsorption between the PA and nanoplastics are free of external perturbations that are caused by the mechanical compression in typical isotherms. The BAM is highly sensitive towards mechanical compression speed and the resultant artifacts are known to cause domain shape alteration in BAM images.[29,30] All data were recorded at 20 $\pm$ 0.6 °C and 31 $\pm$ 10% relative humidity. ImageJ software (version 1.54f) was used to process the BAM images and the data shown are cropped from their original size to portray the regions of highest resolution without any further editing.

2.7 Infrared reflection–absorption spectroscopy

Infrared reflection–absorption spectroscopy (IRRAS) provides surface-sensitive information on the physical and chemical characteristics of surfactant/lipid films spread on water surfaces. This technique is sensitive to changes in the conformational ordering of the lipid chains as well as the orientation and hydration environment of the polar headgroups in condensed states. IRRAS spectra are represented as reflectance–absorbance (RA) and are defined as,

$$\mathrm{RA} = -\log\frac{(R_\mathrm{f})}{(R_0)}$$

where R_f is the reflectance of the surfactant film and R_0 is the reflectance of the bare aqueous solution. The reflectance measurements were obtained using a custom-built optical setup integrated with a Fourier transform infrared spectrometer (Frontier, PerkinElmer) and a liquid-nitrogen-cooled HgCdTe (MCT) detector. The IRRAS setup, featuring two planar gold mirrors mounted on a breadboard, collects reflected light from the surfactant monolayers and bare aqueous solutions at a 48°

incidence angle relative to the surface normal. The setup was optimized to achieve a high signal-to-noise ratio, building on previous research methodologies.[31,32] In general, the negative IRRAS peaks are associated with the film and the positive IRRAS peaks are associated with the aqueous subphase solution. The experiments were performed in Petri dishes as described in the previous section by spreading the lipid solution to desired MMA representative of the tilted condensed phase with or w/o nanoplastics in the solution phase. Each spectrum is an average of 400 scans that were collected in single-beam mode at the spectral region of 4000–450 cm^{-1}. The spectra shown here have been baseline-subtracted in OriginPro 9 by the adjacent-averaging method without using any higher order polynomial. Each spectra shown represents the average of three individual spectrum, with a standard deviation of >2 cm^{-1} reported for each peak. Peak shifts to higher or lower wavenumber in nanoplastic presence are only reported if the values fall outside the range of standard deviation and spectra are only compared against each other if taken on the same day. Experiments were carried out at 19.1 ± 1.0 °C and a lab relative humidity of 30 ± 10%.

3 Results & discussion

3.1 Hydrodynamic diameter and surface charge of the aged nanoplastics

In our control studies using only neat water (pH ∼ 5.8), the hydrodynamic diameter (D_h) of the fragmented aged PS nanoplastics showed a bimodal distribution with two distinct populations. According to the number-weighted particle size distribution, around 85% of the species exhibited an average D_h of ∼104 ± 24 nm, and the remaining of them exhibited an average D_h of ∼375 ± 81 nm, indicating the presence of larger aggregates along with the nanoplastics themselves. This observation is consistent with the zeta potential value of approximately −27.11 ± 4.99 mV, where the large standard deviation indicates potential instability in the suspension, likely due to aggregation of some of the plastic fragments.[33]

In contrast, the nanoplastics in the seawater mimic (pH ∼ 8.3), predominantly formed large aggregates, with an average D_h of ∼430 ± 89 nm. The formation of only larger aggregates is primarily attributed to the coagulation effect of salt ions as the electrostatic repulsion between surface sulfate groups for similar polystyrene nanoplastics have been shown to prevent aggregation at pH conditions ranging from 2.3 to 11.1.[34] At the high ionic strength (IS) of the salt solutions (∼497 mM) in our experimental system, the counter ions likely exerted a strong screening effect, leading to the suppression of electric double layer at the nanoplastic interface and a decreased repulsion between the negatively charged PS nanoplastics.[35] The assumption is supported by the reduced zeta potential value of −13.12 ± 3.11 mV for the aged PS nanoplastics in the sea water mimic (a decrease in surface charge will lead to greater aggregation/instability). Studies by Wang *et al.* on the commercial version of similar PS nanoplastics with surface sulfate groups at a concentration of 20 mg L^{-1} reported the critical coagulation concentrations for NaCl and $CaCl_2$ solutions to be 158.7 mM and 12.2 mM, respectively.[34] Their results stipulate that divalent cations are more effective at shielding the negative surface charge, with aggregation remaining unaffected by co-ions at high IS. It was also suggested that for salt solutions close to critical coagulation concentration or higher, the charge of the PS nanoplastics is fully screened, the energy barrier between the particles is eliminated and the aggregation kinetics reaches a maximum that is independent of salt concentration. Interestingly, the decrease in surface charge of the PS nanoplastics in our sea water mimic is quite comparable with what they observed for natural sea water (−11.3 mV).[34] In contrast, the average D_h of the PS nanoplastics in the sea water mimic of the current study is found to be around 6 times smaller than what was reported by Wang *et al.* for natural sea water.[34] The observed discrepancy in the average D_h could stem from several individual factors, or a combination of them. First, the concentration of PS nanoplastics in their research was approximately four times higher than what we used. This elevated concentration may have promoted greater aggregation at the high ionic strength, leading to larger agglomerates. Second, the solar UV-weathered PS nanoplastics used in our study adopted a more fibrous/flaky morphology, contrasting with the smooth, spherical commercial nanoplastics used in their work. The anisotropic shape and surface deformation of the aged particles could potentially lead to an uneven distribution of charge, resulting in inefficient screening of the electric double layer by salt ions and thus reducing aggregation. Third, their study involved equilibrating the solutions over a longer time scale, which may have allowed the formation of larger aggregates or sediments over time. Fourth, they used natural sea water which is more enriched in natural organic matter (NOM) such as humic substances and other dissolved salt ions that could have potentially promoted greater aggregation.

3.2 Effect of aged PS nanoplastics on surface packing and stability of PA films

As mentioned in the method section, the surface pressure–area (π–A) isotherms of PA on the sea water mimic (termed as proxy sea water, PSW from hereon) undergoes different phase/packing behavior due to changing surface density of the molecules upon compression. Such experimental data provide an initial understanding of how nanoplastics behave at the air–aqueous interface during seasonal marine environmental changes, such as algal blooms, when the concentration of surface-active molecules in the SSML increases over the course of the bloom. The mechanical compression in the isotherms also serves as a good model for the shrinking surface area of a rising sea spray aerosol droplet undergoing evaporation with altitude. As such, any changes in the mechanical stability or molecular organization due to the presence of nanoplastics in the different isotherm phases reflect potential changes in gas uptake, coalescence, and heterogeneous interfacial chemistry at the aerosol surface.

In our experiments, the PA films on the PSW subphase solution revealed their characteristic phase behavior on salt solutions as observed in prior research (Fig. 1a).[13] The PA film underwent a two-dimensional phase transition from the Gas-Tilted Condensed (G-TC) coexistence phase to TC phase at

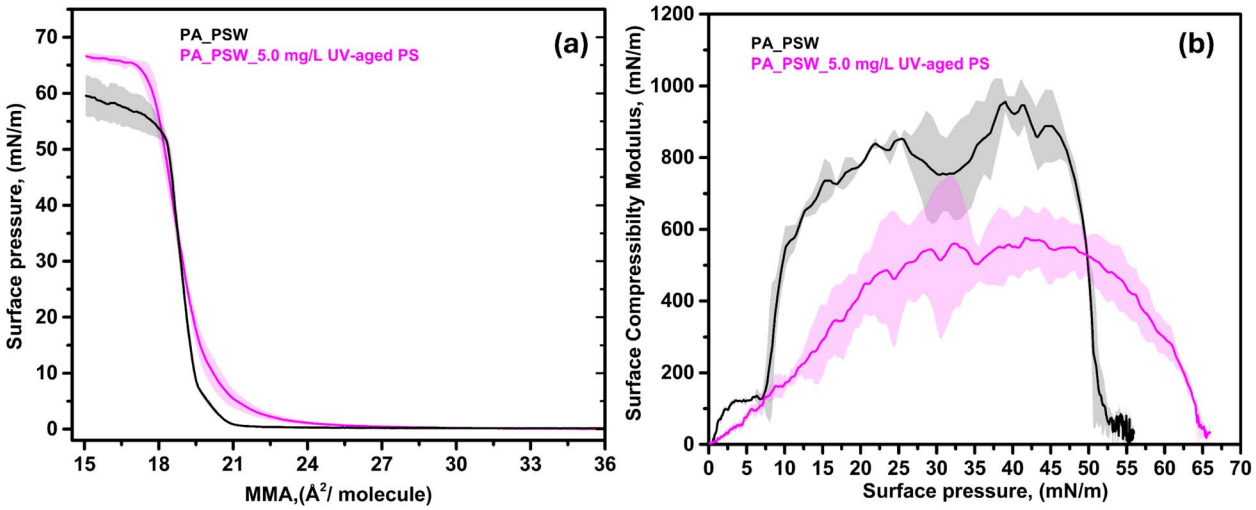

Fig. 1 (a) Surface pressure–area isotherms (b) Surface compressibility modulus of PA film spread on proxy seawater (PSW) subphase solutions with or w/o polystyrene nanoplastics. The shaded areas represent standard deviation (±s).

approximately 21 Å^2 per molecule, regarded as the lift-off point.[25,36,37] Further compression in the TC phase led to the formation of the Untilted Condensed (UC) phase at a surface pressure of approximately 8 mN m^{-1}. It should be noted that both the TC and UC phases make up the condensed state of the isotherm, with the film compressibility decreasing further after the kink observed between them. The system subsequently reached a maximum surface pressure of about 60 mN m^{-1} at the targeted mean molecular area (MMA) of 15 Å^2 per molecule, after passing through a collapse pressure of approximately 51 mN m^{-1}. The high collapse pressure followed by the plateau indicates enhanced stability of the PA film (*i.e.*, resistance to collapsing into 3D structures from the 2D film) on the PSW subphase solution. Such phase behavior in the literature has been attributed to the interaction of the dissociated carboxylate moieties with the salt counter ions. The coulombic repulsion between the negatively charged carboxylate headgroups, along with the formation of contact ion pairs (or solvent-shared/solvent-separated ion pairs) between the carboxylate and Na^+/Ca^{2+}, might contribute to a slow relaxation kinetics.[13,20,38] This, in turn, can impede the transformation of the 2D PA film into a 3D phase, likely due to the increased surface affinity of the lipids in the presence of salt ions.[20] Notably, PA has a surface pK_a of approximately 8.3 at 20 °C, meaning it should be partially deprotonated in our experimental system with a pH of ~8.3.[39,40] However, previous studies have shown that the presence of salt ions at high concentrations like that of our system can lead to complete deprotonation of the carboxylate headgroups.[20,41,42]

Another contributing factor to the high surface pressure plateau can be the intermediate rigidity of the PA film in salt presence. Structural defects within the film would lead to monolayer buckling and protrusions into the subphase solution, known as "giant folds" that can grow in length and amplitude with compression.[13,43] As reported in prior theoretical and experimental studies, these folds are anchored at the lipid monolayer and projects into the solution from few tens to several hundred micrometers.[43,44] At the collapse plateau, the monolayer coexists with these folds and the surface pressure is maintained due to constant number of lipids at a fixed interfacial area.[44] Upon further compression, the giant folds may detach from the monolayer and move freely within the solution phase.[43]

When nanoplastics were introduced in the PSW solution, the shape of the PA isotherm changed, suggesting modifications in the interfacial structure driven by the Brownian movement of dispersed PS aggregates in the seawater environment. The lift-off point increased to ~25 Å^2 per molecule and the transition from the G-TC coexistence phase to the condensed phase became more continuous in nature; the sharp kinks that indicates the formation of TC and UC phases were absent in nanoplastic presence. Such expansion of the isotherm to larger MMA in nanoplastic presence and the subsequent changes in film compressibility hints at diminished rigidity of the film under mechanical compression. A likely explanation is that the aggregated PS nanoplastics undergoing constant Brownian motion disrupt the packing of the surface-deposited lipid film through non-specific interactions. Lipid–nanoplastic complexes may form and incorporate into the surface lipid film, increasing its fluidity (*i.e.*, compressibility upon mechanical compression during the isotherm experiments) due to the relatively weaker interactions between nanoplastics and lipids compared to lipid–lipid cohesion.[45] Interestingly, at higher surface pressures (~30 mN m^{-1}), the PA isotherm in nanoplastic presence overlapped with the previous isotherm for the PSW solution without nanoplastic presence, and further shifted towards decreased molecular area upon compression. This suggests that the previously assumed lipid–nanoplastic complexes, or at least some of them, might have been squeezed out of the interface into the bulk water under symmetric compression. The PA film also collapsed at a higher surface pressure in the presence of the aggregated PS nanoplastics (around ~65 mN m^{-1}), followed by a plateau. This plateau can be attributed to a greater stability of the film at the air–aqueous interface, maintained through the

previously discussed contact/solvent-shared ion pair formation between the carboxylate moiety and Na^+/Ca^{2+} ions with additonal lipid–nanoplastic interactionscontact ion. Such increased collapse pressure of the PA compression isotherm in nanoplastic presence potentially indicates towards changes in hygroscopicity, reactive uptake behavior of the aerosol surface during evaporation in the environment which can eventually affect its ability to act as a CCN or ice nucleating particle.

We further explored the integrity of the PA film in our PSW systems by calculating the isothermal compressibility modulus (Fig. 1b). The compressibility modulus C_s^{-1} is defined as $-A_\pi(\partial\pi/\partial A_\pi)_T$; where A_π is the molecular area at the corresponding π, and a higher value of C_s^{-1} typically corresponds to a more rigid film.[23] For PA on the seawater mimic (without nanoplastics), with increasing surface pressure, two distinct maxima in the compressibility modulus were observed around 5 and 35 mN m^{-1}, corresponding to the TC and UC phases, respectively. In contrast, only a single, broad maximum appeared around 40 mN m^{-1} in the presence of aggregated nanoplastics, corresponding to a more continuous condensed phase with increased compressibility and fluidity, as previously discussed. The compressibility modulus of PA in nanoplastic presence was also slightly lowered compared to the PSW system without nanoplastics, specifically at the low surface pressure region. This suggests diminished intermolecular cohesion among the surface PA molecules, likely due to the intercalation of aggregated PS nanoplastics with the lipid film at the expanded region. The resultant weaker lipid–nanoplastic interactions are consistent with the increased fluidity and compressibility seen at surface pressures upto ~52 mN m^{-1}. At surface pressures above this value, the PA film in nanoplastics presence had an increased compressibility modulus suggesting that the film exhibited higher rigidity, which is consistent with the increased collapse pressure observed in our isotherms.

3.3 Effect of aged PS nanoplastics on morphology and reflectivity of PA films

The altered surface morphology of PA films in nanoplastic presence was visualized using BAM, which is highly sensitive towards variations in refractive index and thickness of the interfacial monolayer. Control BAM images of 5 mg L^{-1} PS nanoplastic-salt solutions (without the presence of PA film) revealed that the PS nanoplastic aggregates tend to accumulate at the air–water interface, likely driven by a combination of Brownian movement and floatation (Fig. S1). This accumulation resulted in the formation of clusters up to 50–100 μm in size at the air–aqueous interface—more than two orders of magnitude larger than the aggregates observed *via* DLS in the solution phase. While the salt ions in the PSW solution promote aggregation, the hydrophobic and buoyant nature of the nanoplastics prevents them from sinking, favoring localization at or near the water surface. Interestingly, some of the regions at the aqueous interface showed similarity to previously reported images of polystyrene nanoparticle monolayers on salt-containing subphase solutions, despite the difference in experimental conditions.[46]

We next investigated how the presence of these aggregated PS nanoplastics changed the optical properties of the film at varying surface density of the PA molecules without external perturbation such as mechanical compression. For that, we chose the G-TC coexistence region (around MMA of 32 $Å^2$ per molecule) as a representative of low surface density state and the condensed region (around MMA of 20 $Å^2$ per molecule) as a representative of high surface density state, respectively. At the G-TC coexistence phase (surface pressure of 0 mN m^{-1}), the film primarily exhibited large, condensed domains in slow motion, interspersed with some dark voids that indicate lipid-poor regions on the PSW solution without nanoplastics (Fig. 2). Previous studies have attributed the formation of such large domains to the condensing effect of salt cations, which promote ordering within the monolayer.[47] The tendency of the film to move without any compression, under the non-equilibrium experimental condition in our drop-casting method, also hints at a low degree of rigidity in the G-TC phase, as discussed in the isotherm studies.

In contrast, the presence of aggregated PS nanoplastics in the solution led to marked transformations in the surface morphology (Fig. 3). The BAM images revealed appearance of bright, high-contrast features resembling vesicles or semi-vesicles that seemed to be attached to the monolayer and moving beneath it.[44] These semielliptical features are analogous to previously imaged giant folds formed during monolayer buckling in the collapse phase, as discussed earlier.[13,43] However, the occurrence of these folds deep within the G-TC region, *i.e.*, well before the collapse, suggests that the aggregated PS nanoplastics in the PSW solution engage in significant interactions with the condensed monolayer. These interactions appear to promote premature folding which is not the typical behavior of PA monolayers on salt-only subphases in the G-TC regime. Despite the presence of such folds, the PA monolayer still remained mobile (albeit slower), suggesting an intermediate level of rigidity within the film arising from the additonal lipid–nanoplastic interactions/complexes. This is illustrated by the tracked movement of a dark void/hole in the monolayer over time (highlighted by the blue shapes in Fig. 3). It should be noted that in case of our BAM studies, no mechanical compression was applied, and as such the intermediate rigidity in nanoplastic presence indicates a higher surface activity (*i.e.*, the non-specific lipid–nanoplastic interactions) in the air–aqueous interface at the respective surface lipid density. As suggested in our isotherm studies, such interactions lead to fluidity in the monolayer during mechanical compression since the lipid–nanoplastic interactions are much weaker than the lipid–lipid interactions and will be more compressible during the symmetric compression. Overall, the findings are consistent with the altered PA isotherm behavior observed in the presence of aggregated nanoplastics during the transition to condensed phases; this further indicates changes in the surface properties of the model aerosol system, with implications for the modified optical albedo of sea spray aerosols incorporating nanoplastics into their structure.

At the condensed phase region (~5 mN m^{-1}), the PA film on salt solution without nanoplastics showed similar large

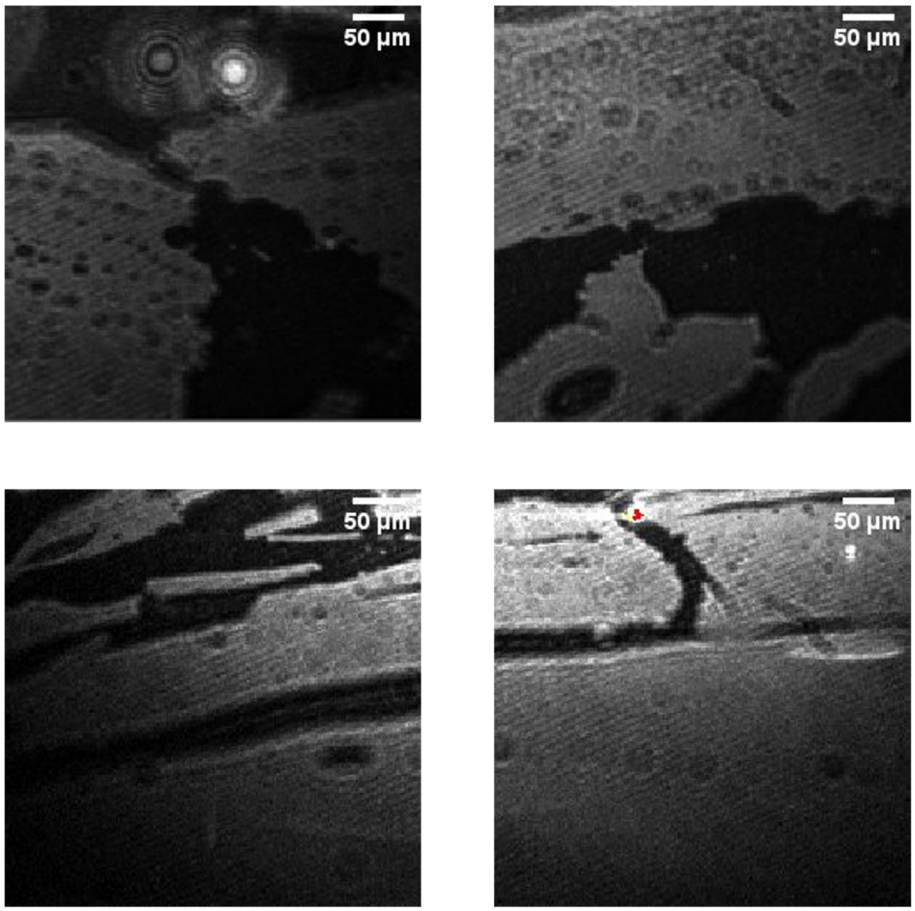

Fig. 2 BAM images of different regions of the PA film in the G-TC phase at ~32 Å^2 per molecule on PSW subphase solution without PS nanoplastics. The images show different domain regions of the dense film due to its temporal mobility with respect to the fixed camera position as described in the method section. (All images are cropped into 400 μm × 400 μm snapshots with 50 μm scale bar).

domains as the G-TC phase (Fig. 4a). However, these condensed domains were predominantly stagnant, hinting at a strongly ordered monolayer at the higher concentration of surface lipids. In the presence of aggregated PS nanoplastics, the surface morphology again showed semi-elliptical features attached to the monolayer, similar to those observed at the G-TC phase under nanoplastic conditions (Fig. 4b). The key difference, though, was the lack of movement: both the monolayer and the folds beneath it appeared mostly passive, with little to no dynamic behavior over time (displayed by lack of movement of the fold marked by yellow shapes). This observation is consistent with the expulsion of lipid–nanoplastic complexes at higher surface pressures assumed in our isotherm analysis; the more rigid monolayer will indeed have lower compressibility, and the surface molecules have the potential to desorb from the monolayer into the bulk under compression.

3.4 Probing the chemical signature of lipid–nanoplastic interactions through IRRAS

To complement the isotherm and BAM results, we probed the chemical structure and molecular organization of the PA film in nanoplastic presence at ~20 Å^2 per molecule (condensed phase) by employing Infrared Reflection–Absorption Spectroscopy (IRRAS). We focused on both the alkyl chain and the headgroup region, as they both are sensitive to perturbations from solution phase interactions. The methylene stretching region at 2800–3000 cm^{-1} is particularly responsive to interfacial changes.[48] In our experiments, we did not observe a peak shift in this region from the presence of aggregated nanoplastics in the PSW solution. The spectra can be found in the SI (Fig. S2 and S3) with appropriate peak assignment based on literature.[49–52] But briefly, the $\nu_s(CH_2)$ and $\nu_{As}(CH_2)$ modes were seen at 2850 cm^{-1} and 2916 cm^{-1} respectively, suggesting all-trans extended surfactant chains that are nearly perpendicular to the aqueous interface (consistent with the highly ordered condensed phase).[50] This hints at a conserved uniform molecular orientation of the hydrocarbon chains of the PA monolayer, even at buckling to the giant folds, as observed in our BAM studies of this particular region in nanoplastic presence. The peak-height intensity ratio of the $\nu_{As}(CH_2)$ and $\nu_s(CH_2)$ modes also remained constant (~1.39), indicating unchanged packing/conformational order among the chains in nanoplastic presence.[50,53] Such rigidity of the PA film is also consistent with the dominance of stronger lipid–lipid interaction assumed in our isotherm analysis for this region. Therefore, it can be concluded

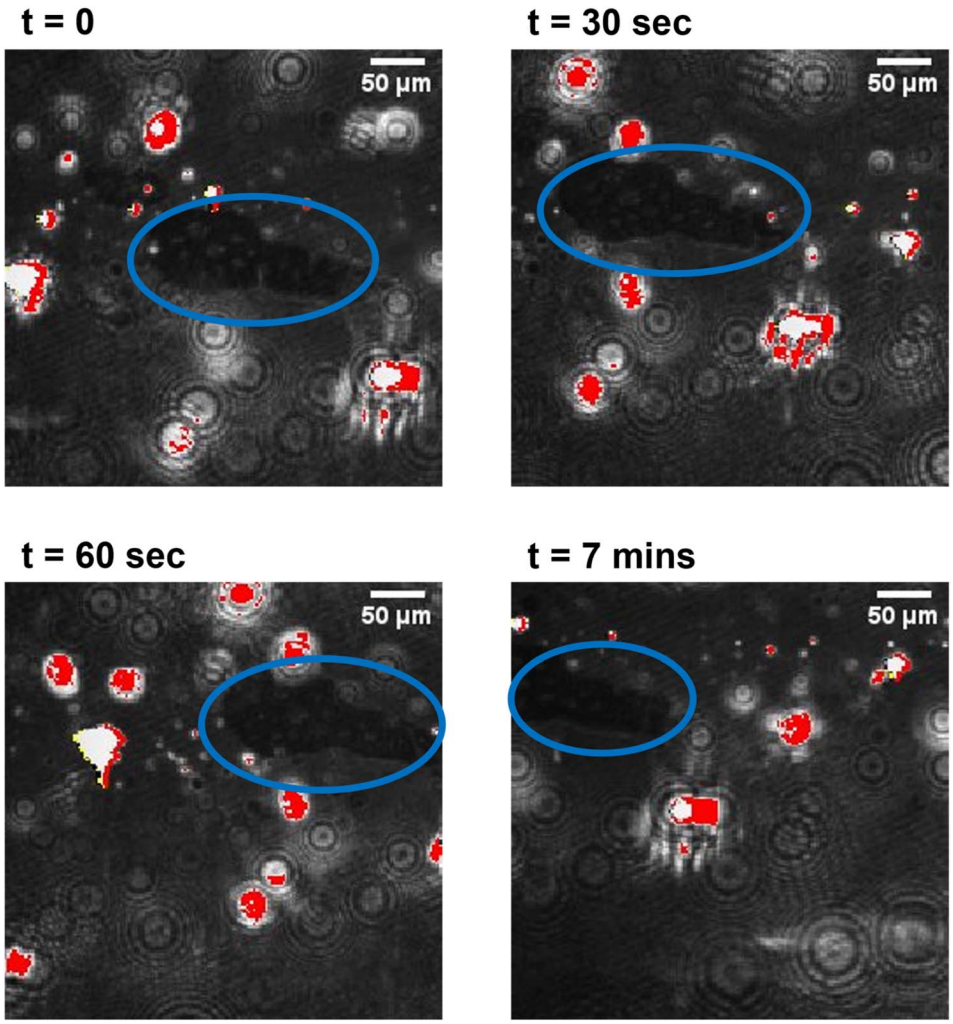

Fig. 3 BAM images of the PA film in the G-TC phase at ~32 Å^2 per molecule on the PSW solution containing aggregated PS nanoplastics. (All images are cropped into 400 μm × 400 μm snapshots with 50 μm scale bar). The images show changes observed as a function of time, with the blue shapes showing the movement of a dark void/hole in the film. The red tint can be attributed to error in refresh rate of the camera or oversaturation at the camera sensor due to higher light reflectivity of the giant folds beneath the film.

that, even though the aggregated PS nanoplastics in PSW solution might disrupt lipid packing at lower surface pressure region (as indicated by the expanded isotherm), they do not disorder the packing structure of the hydrophobic core of the condensed PA film at regions of higher surface pressure. This implies that nanoplastics incorporated into sea spray aerosols during wave-breaking events are unlikely to disrupt the alkyl chain order of insoluble fatty acids at higher altitudes, where continuous evaporation reduces droplet surface area to form highly condensed film. Consistently, the δ (CH_2) or the CH_2 scissoring mode was observed at 1468 cm^{-1} for the PSW subphase solutions with or without nanoplastics (Fig. 5), further suggesting that the *trans*-oriented alkyl chains are packed in a hexagonal subcell.[54] This indicates that the monolayer folding observed in our BAM analysis of this region still maintains the hexagonal lattice packing structure in nanoplastic presence. Taken together, the spectroscopic evidence suggests that in this condensed phase state, despite the hydrophobic nature of the aggregated nanoplastics, they do not disorder the hydrocarbon chains of the surface lipids by direct insertion at the air–aqueous interface or other means, due to the dominance of stronger lipid–lipid interactions. Instead, the nanoplastics likely reside in a subsurface region—beneath the topmost molecular layer—where they remain buoyant with the potential to form lipid–nanoplastic interactions/complexes with the carboxylate headgroup.

The bands in the 1700–1740 cm^{-1} region, typically associated with the C=O stretching vibrations of protonated carbonyl species in PA, were not observed for PSW solutions both in the presence and absence of nanoplastics (change in baseline was within the noise level). This absence suggests that the carboxylic acid headgroups are fully deprotonated under the high-salt concentration of our experimental system at pH 8.3, as seen previously in similar systems.[20,41] Instead, prominent bands corresponding to the symmetric and asymmetric stretching vibrations of the carboxylate (CO_2^-) group were observed at

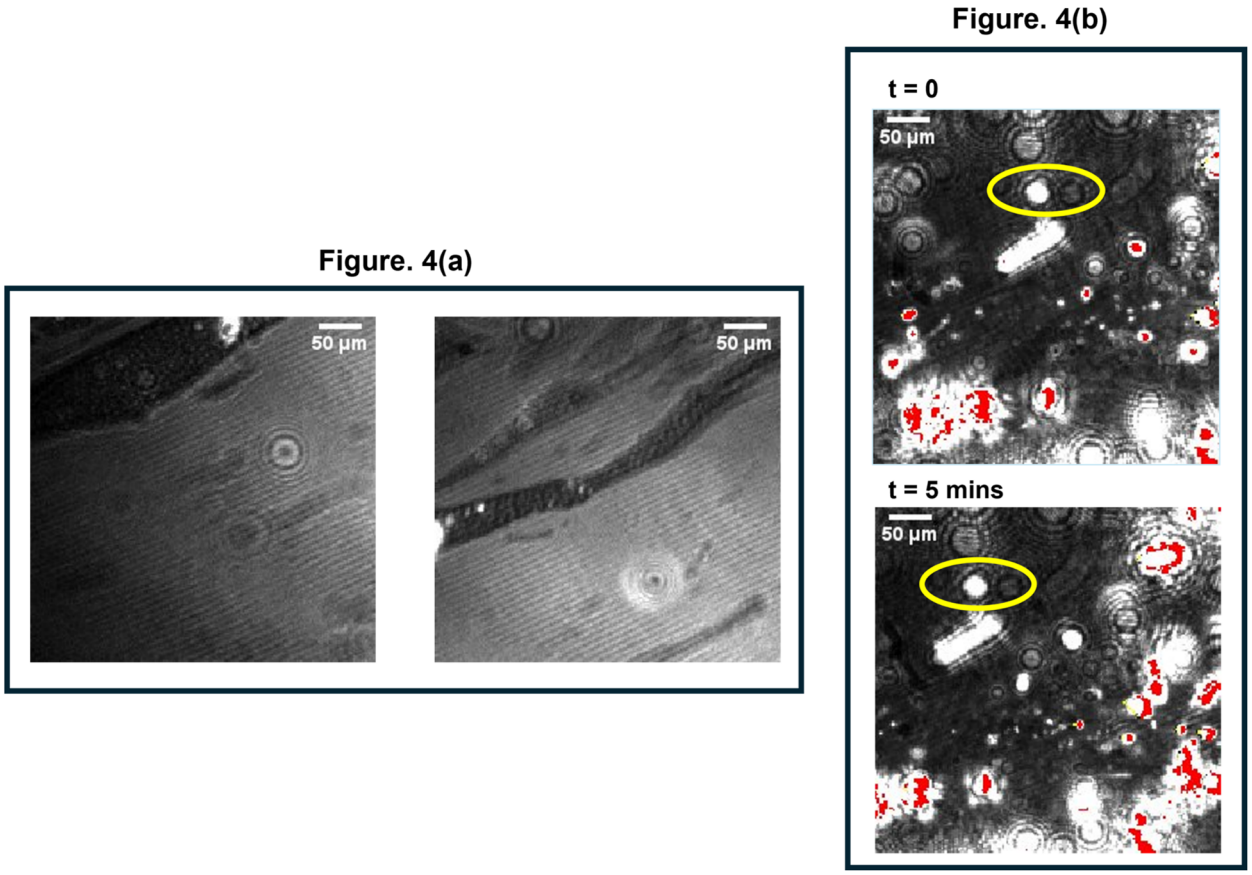

Fig. 4 (a) BAM images of different regions of the mostly stagnant PA film at the condensed phase ~20 Å^2 per molecule on PSW subphase solution without nanoplastics. (b) BAM images of the PA film on the PSW subphase containing aggregated PS nanoplastics. The yellow shapes in the images show only slight movement of the giant folds beneath the monolayer over a longer period of time in the condensed phase. (All images are cropped into 400 μm × 400 μm snapshots with 50 μm scale bar).

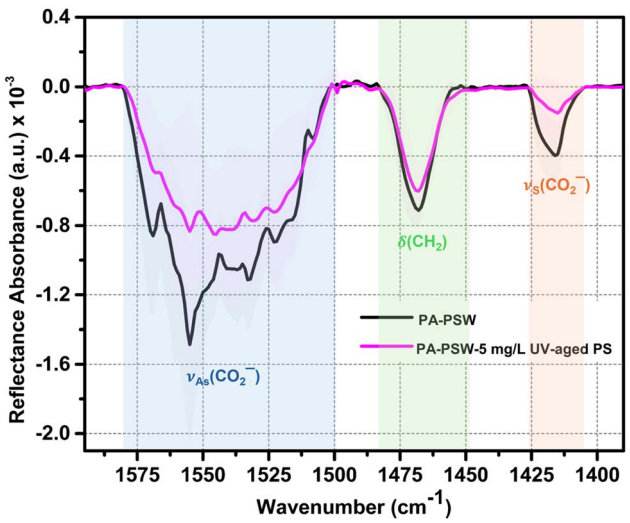

Fig. 5 IRRAS spectra of PA film (~20 Å^2 per molecule) spread on PSW solution subphases (with and w/o aggregated PS nanoplastics) in the 1400–1800 cm^{-1} region.

~1417 cm^{-1} and between 1500–1575 cm^{-1}, respectively, confirming deprotonation at the air–water interface. On average, the IR sensitive $\nu_{As}(CO_2^-)$ stretching appeared to have red shifted in the presence of the aggregated PS nanoplastics whereas the $\nu_s(CO_2^-)$ stretching remained largely unchanged. We further deconvoluted the asymmetric carboxylate stretching region using the built-in Gaussian function in OriginPro and found that the best fit was achieved with three distinct peaks (adj. $R^2 \geq 0.97$), similar to the results reported by Gericke *et al.* in their studies of stearic acid (SA) on a calcium chloride subphase solution.[42] Although SA and palmitic acid (PA) share structural similarities and both are highly insoluble in water, they differ in hydrocarbon chain length—SA being two methylene (–CH_2–) units longer than PA. And while Gericke *et al.* employed a 1 mM $CaCl_2$ solution, the subphase solution in our experimental system contained a significantly higher salt concentration: 10 mM $CaCl_2$ along with 467 mM NaCl.[42] It should also be noted that the 1500–1575 cm^{-1} region in our spectra contained contributions from water vapor bands, likely arising from atmospheric differences in the beam path between the bare and film covered interfacial measurements which were not fully compensated in the logarithmic subtraction process. Nevertheless, the high adj. R^2 and the consistency with more recent literature support the physical interpretation of three distinct $\nu_{As}(CO_2^-)$ peaks in the presence of salt cations.[55]

For the PSW solution without dispersed nanoplastics, the deconvoluted $\nu_{As}(CO_2^-)$ region on average exhibited three peaks

approximately at 1531, 1555, and 1571 cm^{-1} (Fig. S4), closely matching those observed in the individually fitted spectra (data not shown). Notably, these peaks were observed at higher wavenumbers (blue shifted by 3–12 cm^{-1}) compared to those reported by Gericke *et al.*, likely due to the increased ionic strength of our PSW solution given that the alkyl chain orientation in both studies is comparable. Based on their assignments, we conclude that the observed peaks in our system reflect a combination of strong ionic and covalent interactions (potentially arising from monodentate ligand or bidentate chelating/bridging complexes), indicative of cation-induced dehydration at the carboxylate region.[42,56] Previous experimental and theoretical studies suggest that at different concentrations, both Na^+ an Ca^{2+} ions interact with the palmitic acid carboxylate headgroup through solvent-shared and contact ion pairing.[20,57,58] As such, we carried out additional studies to investigate if the cation-carboxylate headgroup interactions observed in our studies have any bias towards the divalent cation and found that at ocean relevant concentrations (where Na^+ is ~47 times of Ca^{2+} in terms of concentration *i.e.*, 467 mM *vs.* 10 mM), despite the divalent charge of Ca^{2+}, the overabundance of Na^+ results in interactions mostly similar to the ones observed in case of NaCl control studies. Although the addition of 10 mM $CaCl_2$ to the 467 mM NaCl subphase occasionally produced slight spectral variations, these effects were not sufficiently consistent or pronounced to support a definitive conclusion. This outcome suggests that the relatively sparse Ca^{2+}–CO_2^- species, compared to the dominant Na^+–CO_2^- complexes, either fail to generate detectable spectral changes in IRRAS or remain masked by the more prevalent Na^+–CO_2^- interactions. Additional discussion on the different control studies is included in the SI (Text S1, and Fig. S5–S7).

Interestingly, in the presence of nanoplastics, the asymmetric carboxylate peaks red-shifted to 1527, 1543, and 1559 cm^{-1}, respectively (Fig. S8). The first two peaks align closely with those reported by Gericke *et al.* and we attribute the observed red shifts primarily to decreased carboxylate interactions with salt cations rather than direct interaction/binding with the negatively charged nanoplastics present in our PSW solution. Although zeta potential measurements indicate that the PS nanoplastics retain a net negative surface charge (−13.12 ± 3.11 mV), their surfaces are effectively screened in the high-ionic-strength PSW medium, which contains critical coagulation concentrations of both NaCl and $CaCl_2$.[34] This screening should drastically reduce the range of their electrostatic potential, rendering it negligible beyond the Debye length. As a result, significant electrostatic repulsion between the nanoplastics and the negatively charged carboxylate headgroups is unlikely. The assumption is consistent with the observed red shifts; if repulsive interactions with the carboxylate headgroups were dominant, a blue shift would be expected instead.[9]

The 1543 cm^{-1} peak (observed at 1542 cm^{-1} by Gericke *et al.*) is typically attributed to "hydrated" or "unassociated" carboxylate anions. This red shift suggests increased hydration at the carboxylate region in the presence of nanoplastics, likely due to a reduction in the number of molecular species that are characterized by direct interactions between cations and the carboxylate headgroups. This interpretation is further supported by our zeta potential measurements, which indicate suppression of the electric double layer (EDL) at the nanoplastic interface—an effect attributed to strong ionic screening. Such an occurrence would potentially reduce the number of cations available in the PSW solution for complexation with the PA headgroups, especially the Ca^{2+} ions, due to their higher affinity towards the negatively charged polystyrene nanoplastics. This suggests that, although the aggregated PS nanoplastics may not directly bind to the carboxylate groups, they likely diffuse into the subsurface region beneath the air–aqueous interface and influence the hydration of the polar headgroup region by scavenging cations from the surrounding solvation environment. Based on previous literature, the peak at 1559 cm^{-1} might be hinting at an ionic Ca^{2+}/Na^+: –CO_2^- interaction (*i.e.*, contact ion pairing), with the 1528 cm^{-1} peak suggesting partial covalent character of some of the carboxylate-metal interactions due to a solvent-shared binding environment.[20,42,57] Notably, the prominent positive feature around 1650 cm^{-1} (Fig. S9) corresponds to the bending mode of water from the aqueous solution subphase and is typical of classical IRRAS spectra of thin films at the air–water interface. This arises from the change in the refractive index of water in this wavelength region and cannot be avoided.[42]

Our spectroscopic results are still quite consistent with the previously assumed lipid–nanoplastic complexes/interactions, with the spectroscopic evidence pointing towards a cation-mediated interaction between the nanoplastics and the lipid monolayer at the condensed state, likely occurring in the subsurface region beneath the air–aqueous interface as mentioned. In this subsurface, nanoplastics do not perturb the packing order of the hydrophobic chains but their influence on the polar headgroup region still exerts substantial impact on the interfacial structure, as observed in our isotherm and BAM studies. The findings give insight into a potential mechanism that may compete with different sedimentation processes in the ocean surface and lead to nanoplastic enrichment at the sea surface microlayer. The chemical interactions observed also demonstrate a possible pathway for nanoplastic interaction with the surface organic film in sea spray aerosols resembling reverse micelles.

4 Conclusions & environmental implications

This study demonstrates that UV-aged polystyrene nanoplastics show distinct aggregation behavior in a proxy ocean saline environment and significantly influence the interfacial structure and morphology of palmitic acid films, a representative fatty acid that is commonly found at marine interfaces such as sea surface microlayer (SSML) and sea spray aerosols (SSAs). Isotherm analysis indicated disrupted packing and altered compressibility, particularly at higher surface pressure or higher surface density regions due to the presence of aggregated nanoplastics in the saline subphase. The results indicate the existence of nanoplastic–lipid interactions at different surface

densities of marine organics at the sea surface microlayer as well as at the shrinking surface of aerosol droplets during evaporation in the environment. Complementary BAM imaging across varying PA surface densities showed morphological changes stemming from monolayer buckling, potentially responsible for the observed changes in the isotherm compressibility. Despite these morphological changes, IRRAS results indicate that the PA hydrocarbon chains remain well-ordered at the condensed phase in our marine interface mimic. Further spectroscopic analysis suggests that the aggregated nanoplastics likely reside beneath the PA films, where their negative surface charge drives ion redistribution in the interfacial region and modifies the hydration environment around the carboxylate headgroups. The resultant cation-mediated, subsurface headgroup–nanoplastic interactions can modulate the PA monolayer environment without disrupting the hydrophobic core ordering, as observed across our isotherm and BAM data.

Although the nanoplastic concentrations used in this study exceed current levels detected in remote surface waters, they provide insight into potential impacts in regions of elevated plastic pollution, such as coastal and semi-enclosed marine systems subjected to high anthropogenic influence. Our findings underscore that nanoplastics can influence the chemistry of the sea surface microlayer, highlighting their potential to become a persistent modifier of the SSML and SSA composition. As environmental plastic waste continues to fragment into smaller particles and accumulate in these surface oceans, the likelihood of nanoplastics interfering with natural air–sea exchange, pollutant transport, and microbial activity in the SSML becomes increasingly relevant. During wave generation and breaking, structural changes in the SSML lead to the formation of SSAs that incorporate nanoplastics accumulated in or near the microlayer, thereby altering the chemical makeup of aerosols entering the atmosphere. Our results demonstrate that nanoplastics incorporated within SSA droplets can modify their surface properties during atmospheric evaporation, potentially changing hygroscopicity, coalescence, and light scattering behavior, which directly and indirectly affect the cloud-nucleating ability and radiative forcing. Consequently, this emerging pathway of anthropogenic influence on atmospherically relevant aqueous interfaces needs to be acknowledged and integrated into future environmental studies such as marine aerosol research and climate models.

In summary, while nanoplastics have largely been studied in the context of marine pollution and ecological toxicity, our work illustrates that their impact likely extends into the atmospheric system—with the potential to affect cloud properties and climate regulation due to their incorporation into SSAs and subsequent surface morphology changes. Importantly, the effects we observe confirm that nanoplastics are not just passive contaminants but are active players in ocean–atmosphere exchange processes. Their role in altering interfacial chemistry and morphology in aqueous interfaces such as SSML and SSA underscores a need to incorporate plastic pollution into our understanding of the marine boundary layer. As such, future models of marine aerosol formation and climate interactions should consider the influence of nanoplastics in the composition and functionality of the sea surface microlayer, and optical albedo, hygroscopicity of the generated SSAs, especially under conditions of rising plastic load and evolving ocean chemistry. Doing so will improve the accuracy of predictions related to aerosol–cloud interactions and regional climate behavior, thereby supporting the development of evidence-based regulatory frameworks aimed at mitigating the atmospheric and oceanic impacts of micro- and nanoplastic pollution in near future.

Author contributions

Shamma Jabeen Proma: project lead, data collection, data analysis, literature review, manuscript writing & preparation. Biswajit Biswas: sample preparation, data analysis, data plotting. Shahin Ahmed Sujon: sample preparation, data analysis. Kyle J. Moor: data analysis, manuscript editing. Janice Brahney: data analysis, manuscript editing. Heather C. Allen: principal investigator, data analysis, manuscript writing & preparation.

Conflicts of interest

There are no conflicts to declare.

Data availability

Data will be made available on request.

Supplementary information is available. See DOI: **https://doi.org/10.1039/d5ea00075k**.

Acknowledgements

This research was supported by the Herbert W. Hoover foundation through grant no. GR 130261. The authors would like to thank Dr Blair Rist from the Schultz Group in the Department of Chemistry & Biochemistry, The Ohio State University, for assisting with the DLS and Zeta Potential Measurements. We are also grateful to Dr Jessica Clark and Dr Nicole North (Alumni, Allen Lab) for their guidance and support throughout the project.

References

1 D. Allen, S. Allen, S. Abbasi, A. Baker, M. Bergmann, J. Brahney, T. Butler, R. A. Duce, S. Eckhardt, N. Evangeliou, *et al.*, Microplastics and nanoplastics in the marine-atmosphere environment, *Nat. Rev. Earth Environ.*, 2022, **3**(6), 393–405, DOI: **10.1038/s43017-022-00292-x**.

2 A. I. Catarino, M. C. León, Y. Li, S. Lambert, M. Vercauteren, J. Asselman, C. R. Janssen, G. Everaert and M. De Rijcke, Micro- and nanoplastics transfer from seawater to the atmosphere through aerosolization under controlled laboratory conditions, *Mar. Pollut. Bull.*, 2023, **192**, 115015, DOI: **10.1016/j.marpolbul.2023.115015**.

3 A. Gangula, T. Chhetri, M. Atty, B. Shanks, R. Kannan, A. Upendran and Z. Afrasiabi, Unaccounted Microplastics in the Outlet of Wastewater Treatment Plants—Challenges

and Opportunities, *Processes*, 2023, **11**(3), 810, DOI: **10.3390/pr11030810**.

4 S. Bucci, C. Richon and L. Bakels, Exploring the Transport Path of Oceanic Microplastics in the Atmosphere, *Environ. Sci. Technol.*, 2024, **58**(32), 14338–14347, DOI: **10.1021/acs.est.4c03216**.

5 E. v. Sebille, C. Wilcox, L. Lebreton, N. Maximenko, B. D. Hardesty, J. A. v. Franeker, M. Eriksen, D. Siegel, F. Galgani and K. Lavender Law, A global inventory of small floating plastic debris, *Environ. Res. Lett.*, 2015, **10**, 124006.

6 S. Moon, L. M. A. Martin, S. Kim, Q. Zhang, R. Zhang, W. Xu and T. Luo, Direct observation and identification of nanoplastics in ocean water, *Sci. Adv.*, **10**(4), eadh1675, DOI: **10.1126/sciadv.adh1675**.

7 P. S. Liss, Microplastics: All up in the air?, *Mar. Pollut. Bull.*, 2020, **153**, 110952, DOI: **10.1016/j.marpolbul.2020.110952**.

8 D. Materić, M. Peacock, J. Dean, M. Futter, T. Maximov, F. Moldan, T. Röckmann and R. Holzinger, Presence of nanoplastics in rural and remote surface waters, *Environ. Res. Lett.*, 2022, **17**(5), 054036, DOI: **10.1088/1748-9326/ac68f7**.

9 E. M. Adams, *Spectroscopic Studies of Atmospherically- and Biologically-Relevant Interfaces: Lipids, Ions, and Interfacial Water Structure*, The Ohio State University, 2016, **http://rave.ohiolink.edu/etdc/view?acc_num=osu1480608026126993**.

10 S. Lambert, M. Vercauteren, A. I. Catarino, Y. Li, J. Van Landuyt, N. Boon, G. Everaert, M. De Rijcke, C. R. Janssen and J. Asselman, Aerosolization of micro- and nanoplastics *via* sea spray: Investigating the role of polymer type, size, and concentration, and potential implications for human exposure, *Environ. Pollut.*, 2024, **351**, 124105, DOI: **10.1016/j.envpol.2024.124105**.

11 C. Harb, N. Pokhrel and H. Foroutan, Quantification of the Emission of Atmospheric Microplastics and Nanoplastics *via* Sea Spray, *Environ. Sci. Technol. Lett.*, 2023, **10**(6), 513–519, DOI: **10.1021/acs.estlett.3c00164**.

12 D. B. Shaw, Q. Li, J. K. Nunes and L. Deike, Ocean emission of microplastic, *PNAS Nexus*, 2023, **2**(10), pgad296, DOI: **10.1093/pnasnexus/pgad296**.

13 K. A. Carter-Fenk and H. C. Allen, Collapse Mechanisms of Nascent and Aged Sea Spray Aerosol Proxy Films, *Atmosphere*, 2018, **9**, 503.

14 J. Haywood and O. Boucher, Estimates of the direct and indirect radiative forcing due to tropospheric aerosols: A review, *Rev. Geophys.*, 2000, **38**(4), 513–543, DOI: **10.1029/1999RG000078**.

15 D. P. Veghte, M. B. Altaf and M. A. Freedman, Size dependence of the structure of organic aerosol, *J. Am. Chem. Soc.*, 2013, **135**(43), 16046–16049, DOI: **10.1021/ja408903g**.

16 M. B. Altaf, A. Zuend and M. A. Freedman, Role of nucleation mechanism on the size dependent morphology of organic aerosol, *Chem. Commun.*, 2016, **52**(59), 9220–9223, DOI: **10.1039/C6CC03826C**.

17 M. B. Altaf, D. D. Dutcher, T. M. Raymond and M. A. Freedman, Effect of Particle Morphology on Cloud Condensation Nuclei Activity, *ACS Earth Space Chem.*, 2018, **2**(6), 634–639, DOI: **10.1021/acsearthspacechem.7b00146**.

18 M. A. Freedman, Phase Separation in Organic Aerosol, *Chem. Soc. Rev.*, 2017, **46**, 7694.

19 X. Zhu, J. Konik and H. Kaufman, The knowns and unknowns in our understanding of how plastics impact climate change: a systematic review, *Front. Environ. Sci.*, 2025, **13**, DOI: **10.3389/fenvs.2025.1563488**.

20 E. M. Adams, B. A. Wellen, R. Thiraux, S. K. Reddy, A. S. Vidalis, F. Paesani and H. C. Allen, Sodium–Carboxylate Contact Ion Pair Formation Induces Stabilization of Palmitic Acid Monolayers at High PH, *Phys. Chem. Chem. Phys.*, 2017, **19**, 10481.

21 M. G. Vazquez de Vasquez, M. M. Rogers, K. A. Carter-Fenk and H. C. Allen, Discerning Poly- and Monosaccharide Enrichment Mechanisms: Alginate and Glucuronate Adsorption to a Stearic Acid Sea Surface Microlayer, *ACS Earth Space Chem.*, 2022, **6**(6), 1581.

22 D. J. Donaldson and V. Vaida, The Influence of Organic Films at the Air–Aqueous Boundary on Atmospheric Processes, *Chem. Rev.*, 2006, **106**(4), 1445–1461, DOI: **10.1021/cr040367c**.

23 S. J. Proma, B. Biswas, M. Y. Noor and H. C. Allen, Nanoplastic-Induced Disruption of DPPC and Palmitic Acid Films: Implications for Membrane Integrity, *Environ. Sci. Technol.*, 2025, **59**(21), 10215–10226, DOI: **10.1021/acs.est.5c04793**.

24 S. A. Sujon, A. Fabiszak, J. Brahney and K. J. Moor, Wavelength Sensitive Plastic Photodissolution: Elucidating Quantum Yield Trends for Solar Activation Spectra, *Environ. Sci. Technol.*, 2024, **58**(52), 23138.

25 G. L. Gaines, Thermodynamic relationships for mixed insoluble monolayers, *J. Colloid Interface Sci.*, 1966, **21**(3), 315.

26 D. Y. Kwok, B. Tadros, H. Deol, D. Vollhardt, R. Miller, M. A. Cabrerizo-Vílchez and A. W. Neumann, Axisymmetric Drop Shape Analysis as a Film Balance: Rate Dependence of the Collapse Pressure and Molecular Area at Close Packing of 1-Octadecanol Monolayers, *Langmuir*, 1996, **12**(7), 1851.

27 H. Z. Castada, *Brewster Angle Microscopy Study of Model Lung Surfactant Systems at the Air-Water and Air-Physiological Buffer Interfaces*, Master's thesis, Ohio State University, 2010, **http://rave.ohiolink.edu/etdc/view?acc_num=osu1281642097**.

28 J. F. Neal, W. Zhao, A. J. Grooms, A. H. Flood and H. C. Allen, Arginine–Phosphate Recognition Enhanced in Phospholipid Monolayers at Aqueous Interfaces, *J. Phys. Chem. C*, 2018, **122**, 26362.

29 C. W. McConlogue and T. K. Vanderlick, A Close Look at Domain Formation in DPPC Monolayers, *Langmuir*, 1997, **13**(26), 7158.

30 K. J. Klopfer and T. K. Vanderlick, Isotherms of Dipalmitoylphosphatidylcholine (DPPC) Monolayers:

Features Revealed and Features Obscured, *J. Colloid Interface Sci.*, 1996, **182**(1), 220.

31 C. R. Flach, A. Gericke and R. Mendelsohn, Quantitative Determination of Molecular Chain Tilt Angles in Monolayer Films at the Air/Water Interface: Infrared Reflection/Absorption Spectroscopy of Behenic Acid Methyl Ester, *J. Phys. Chem. B*, 1997, **101**, 58.

32 X. Du, W. Miao and Y. Liang, IRRAS Studies on Chain Orientation in the Monolayers of Amino Acid Amphiphiles at the Air–Water Interface Depending on Metal Complex and Hydrogen Bond Formation with the Headgroups, *J. Phys. Chem. B*, 2005, **109**(15), 7428.

33 V. Selvamani, Chapter 15 - Stability Studies on Nanomaterials Used in Drugs. In *Characterization and Biology of Nanomaterials for Drug Delivery*, Mohapatra, S. S., Ranjan, S., Dasgupta, N., Mishra, R. K., Thomas, S., Elsevier, 2019, pp. 425–444.

34 J. Wang, X. Zhao, A. Wu, Z. Tang, L. Niu, F. Wu, F. Wang, T. Zhao and Z. Fu, Aggregation and stability of sulfate-modified polystyrene nanoplastics in synthetic and natural waters, *Environ. Pollut.*, 2021, **268**, 114240, DOI: **10.1016/j.envpol.2020.114240**.

35 D. Lin, S. Drew Story, S. L. Walker, Q. Huang and P. Cai, Influence of extracellular polymeric substances on the aggregation kinetics of TiO2 nanoparticles, *Water Res.*, 2016, **104**, 381–388, DOI: **10.1016/j.watres.2016.08.044**.

36 G. C. Nutting and W. D. Harkins, Pressure–Area Relations of Fatty Acid and Alcohol Monolayers, *J. Am. Chem. Soc.*, 1939, **61**(5), 1180–1187, DOI: **10.1021/ja01874a050**.

37 A. Fischer and E. Sackmann, Electron microscopy and electron diffraction study of coexisting phases of pure and mixed monolayers transferred onto solid substrates, *J. Colloid Interface Sci.*, 1986, **112**(1), 1–14, DOI: **10.1016/0021-9797(86)90064-0**.

38 A. Angelova, D. Vollhardt and R. Ionov, 2D–3D Transformations of Amphiphilic Monolayers Influenced by Intermolecular Interactions: A Brewster Angle Microscopy Study, *J. Phys. Chem. B*, 1996, **100**, 10710.

39 Y. B. Vysotsky, E. S. Kartashynska, D. Vollhardt and V. B. Fainerman, Surface pKa of Saturated Carboxylic Acids at the Air/Water Interface: A Quantum Chemical Approach, *J. Phys. Chem. C*, 2020, **124**(25), 13809.

40 J. R. Kanicky, A. F. Poniatowski, N. R. Mehta and D. O. Shah, Cooperativity Among Molecules at Interfaces in Relation to Various Technological Processes: Effect of Chain Length on pKa of Fatty Acid Salt Solutions, *Langmuir*, 2000, **16**, 172.

41 J. F. Neal, M. M. Rogers, M. A. Smeltzer, K. A. Carter-Fenk, A. J. Grooms, M. M. Zerkle and H. C. Allen, Sodium Drives Interfacial Equilibria for Semi-Soluble Phosphoric and Phosphonic Acids of Model Sea Spray Aerosol Surfaces, *ACS Earth Space Chem.*, 2020, **4**, 1549.

42 A. Gericke and H. Hühnerfuss, The effect of cations on the order of saturated fatty acid monolayers at the air-water interface as determined by infrared reflection-absorption spectrometry, *Thin Solid Films*, 1994, **245**(1), 74–82, DOI: **10.1016/0040-6090(94)90880-X**.

43 C. Ybert, W. Lu, G. Möller and C. M. Knobler, Collapse of a Monolayer by Three Mechanisms, *J. Phys. Chem. B*, 2002, **106**(8), 2004–2008, DOI: **10.1021/jp013173z**.

44 S. Baoukina, L. Monticelli, H. J. Risselada, S. J. Marrink and D. P. Tieleman, The molecular mechanism of lipid monolayer collapse, *Proc. Natl. Acad. Sci. U. S. A.*, 2008, **105**(31), 10803–10808, DOI: **10.1073/pnas.0711563105**.

45 E. Guzmán, L. Liggieri, E. Santini, M. Ferrari and F. Ravera, Influence of silica nanoparticles on phase behavior and structural properties of DPPC–Palmitic acid Langmuir monolayers, *Colloids Surf. A Physicochem. Eng. Asp.*, 2012, **413**, 280.

46 A. Bykov, O. Milyaeva, A. Akentiev, M. Panaeva, N. Isakov, R. Miller and B. Noskov, Impact of Polymer Nanoparticles on DPPC Monolayer Properties, *Colloid Interface*, 2022, **6**, 28, DOI: **10.3390/colloids6020028**.

47 E. M. Adams and H. C. Allen, Palmitic Acid on Salt Subphases and in Mixed Monolayers of Cerebrosides: Application to Atmospheric Aerosol Chemistry, *Atmosphere*, 2013, **4**, 315.

48 P. Garidel, B. Fölting, I. Schaller and A. Kerth, The microstructure of the stratum corneum lipid barrier: Mid-infrared spectroscopic studies of hydrated ceramide:palmitic acid:cholesterol model systems, *Biophys. Chem.*, 2010, **150**(1), 144.

49 D. E. Gragson, B. M. McCarty and G. L. Richmond, Ordering of Interfacial Water Molecules at the Charged Air/Water Interface Observed by Vibrational Sum Frequency Generation, *J. Am. Chem. Soc.*, 1997, **119**(26), 6144–6152, DOI: **10.1021/ja962277y**.

50 S. Cheng, L. Du and C. George, Understanding the Interfacial Behavior of Typical Perfluorocarboxylic Acids at Surfactant-Coated Aqueous Interfaces, *J. Geophys. Res. Atmos.*, 2020, **125**(13), e2019JD032182.

51 M. Xu, N. T. Tsona, S. Cheng, J. Li and L. Du, Unraveling interfacial properties of organic-coated marine aerosol with lipase incorporation, *Sci. Total Environ.*, 2021, **782**, 146893, DOI: **10.1016/j.scitotenv.2021.146893**.

52 R. Lu, W. Gan, B.-h. Wu, Z. Zhang, Y. Guo and H.-f. Wang, C–H Stretching Vibrations of Methyl, Methylene and Methine Groups at the Vapor/Alcohol (n = 1–8) Interfaces, *J. Phys. Chem. B*, 2005, **109**(29), 14118–14129, DOI: **10.1021/jp051565q**.

53 A. C. Machado and L. Caseli, Interaction of nitrofurantoin with lipid langmuir monolayers as cellular membrane models distinguished with tensiometry and infrared spectroscopy, *Colloids Surf., B*, 2020, **188**, 110794, DOI: **10.1016/j.colsurfb.2020.110794**.

54 A. Gericke, A. V. Michailov and H. Hühnerfuss, Polarized external infrared reflection-absorption spectrometry at the air/water interface: Comparison of experimental and theoretical results for different angles of incidence, *Vib. Spectrosc.*, 1993, **4**(3), 335–348, DOI: **10.1016/0924-2031(93)80007-3**.

55 S. Li, L. Du, Z. Wei and W. Wang, Aqueous-phase aerosols on the air-water interface: Response of fatty acid Langmuir monolayers to atmospheric inorganic ions, *Sci. Total*

Environ., 2017, **580**, 1155–1161, DOI: 10.1016/j.scitotenv.2016.12.072.

56 E. M. Adams, C. B. Casper and H. C. Allen, Effect of Cation Enrichment on Dipalmitoylphosphatidylcholine (DPPC) Monolayers at the Air-Water Interface, *J. Colloid Interface Sci.*, 2016, **478**, 353.

57 M. G. Vazquez de Vasquez, B. A. Wellen Rudd, M. D. Baer, E. E. Beasley and H. C. Allen, Role of Hydration in Magnesium *versus* Calcium Ion Pairing with Carboxylate: Solution and the Aqueous Interface, *J. Phys. Chem. B*, 2021, **125**(40), 11308–11319, DOI: 10.1021/acs.jpcb.1c06108.

58 C. Y. Tang and H. C. Allen, Ionic Binding of Na^+ *versus* K^+ to the Carboxylic Acid Headgroup of Palmitic Acid Monolayers Studied by Vibrational Sum Frequency Generation Spectroscopy, *J. Phys. Chem. A*, 2009, **113**, 7383.